

# NJC

Accepted Manuscript

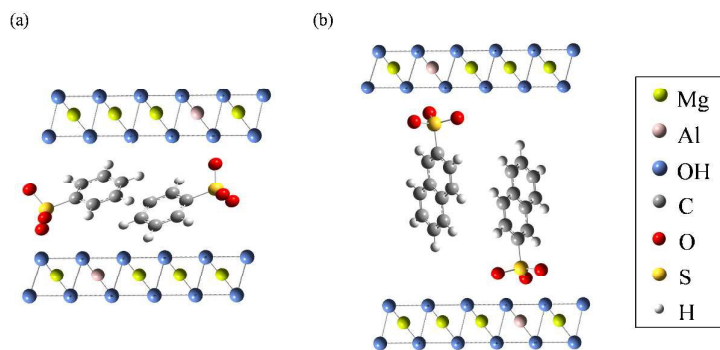


This is an *Accepted Manuscript*, which has been through the Royal Society of Chemistry peer review process and has been accepted for publication.

*Accepted Manuscripts* are published online shortly after acceptance, before technical editing, formatting and proof reading. Using this free service, authors can make their results available to the community, in citable form, before we publish the edited article. We will replace this *Accepted Manuscript* with the edited and formatted *Advance Article* as soon as it is available.

You can find more information about *Accepted Manuscripts* in the [Information for Authors](#).

Please note that technical editing may introduce minor changes to the text and/or graphics, which may alter content. The journal's standard [Terms & Conditions](#) and the [Ethical guidelines](#) still apply. In no event shall the Royal Society of Chemistry be held responsible for any errors or omissions in this *Accepted Manuscript* or any consequences arising from the use of any information it contains.



Both (a) benzenesulfonate and (b) 2-naphthalenesulfonate intercalated in the Mg–Al LDH tend to orient perpendicularly as concentration increases.

1 **Kinetics and equilibrium studies on the removal of aromatic sulfonates from**  
2 **aqueous solution by Mg–Al oxide**

3

4 Tomohito Kameda\*, Mami Umetsu, Toshiaki Yoshioka

5 Graduate School of Environmental Studies, Tohoku University, 6-6-07 Aoba, Aramaki,

6 Aoba-ku, Sendai 980-8579, Japan

7

8 \*Corresponding author

9 Tel: +81-22-795-7212; Fax: +81-22-795-7212

10 E-mail: kameda@env.che.tohoku.ac.jp

11

12

13

## 1 Abstract

2 Mg–Al oxide, which was obtained via the thermal decomposition of Mg–Al  
3 layered double hydroxides (LDHs) intercalated with  $\text{CO}_3^{2-}$  ( $\text{CO}_3\cdot\text{Mg–Al}$  LDH), was  
4 confirmed to take up benzenesulfonate ( $\text{BS}^-$ ) and 2-naphthalenesulfonate ( $\text{NS}^-$ ) in  
5 aqueous solution. The removal of  $\text{BS}^-$  or  $\text{NS}^-$ , which can be described by  
6 pseudo-first-order reaction kinetics, proceeded under chemical reaction control. This  
7 process followed a Langmuir-type adsorption; the maximum and equilibrium adsorption  
8 constants for  $\text{NS}^-$  were larger than those for  $\text{BS}^-$ . Our results suggests that the Mg–Al  
9 oxide reacts more favorably with aromatic sulfonates with lower charge density and that  
10 the effect of hydrophobic interactions is larger than that of electrostatic interactions. In  
11 the initial reaction stage, Mg–Al oxide rehydrates and combines with an aromatic  
12 sulfonate to reconstruct the LDH structure; then, the aromatic sulfonates interact in  
13 aqueous solution through hydrophobic interactions, facilitating their removal by the  
14 Mg–Al oxide. Because the attraction of  $\text{NS}^-$  molecules is stronger than that of  $\text{BS}^-$   
15 molecules, the removal of  $\text{NS}^-$  by the Mg–Al oxide was found to be more efficient than  
16 that of  $\text{BS}^-$ .

17

18

1

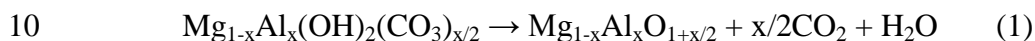
2

3

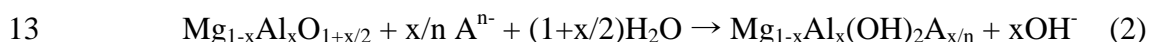
4

## 1 Introduction

2 Mg–Al layered double hydroxides (Mg–Al LDHs) are typically represented by  
 3 the formula  $[\text{Mg}^{2+}_{1-x}\text{Al}^{3+}_x(\text{OH})_2](\text{A}^{n-})_{x/n} \cdot m\text{H}_2\text{O}$ , where  $x$  is the  $\text{Al}^{3+}/(\text{Mg}^{2+} + \text{Al}^{3+})$  molar  
 4 ratio ( $0.20 \leq x \leq 0.33$ ), and  $\text{A}^{n-}$  is an anion such as  $\text{CO}_3^{2-}$  or  $\text{Cl}^-$ .<sup>1-4</sup> They consist of a stack  
 5 of  $\text{Al}^{3+}$ -bearing brucite-like octahedral layers in which the charge of the positive layer is  
 6 neutralized by the interlayer anions. The interlayer space is also occupied by water  
 7 molecules present in the hydration shells of these intercalated anions. Mg–Al LDHs  
 8 intercalated with  $\text{CO}_3^{2-}$  ( $\text{CO}_3$ ·Mg–Al LDH) can be converted into Mg–Al oxides by  
 9 calcination at 450–800 °C, as expressed by Equation 1:



11 The Mg–Al oxide can then rehydrate and combine with anions to reconstruct the LDH  
 12 structure:



14 Recently, Mg–Al oxides have been used to remove organic anions such as Acid Orange  
 15 10, Acid Blue, and methyl orange from aqueous solution.<sup>5-7</sup> The adsorption process in the  
 16 removal of Acid Orange 10 follows a Langmuir model and can be represented by  
 17 pseudo-second-order reaction kinetics.<sup>5</sup> Mg–Al oxide was found to be superior to  
 18 activated carbon for the removal of Acid Orange 10.<sup>5,8</sup> In the removal of inorganic anions

1 by Mg-Al LDH and Mg-Al oxide, an anion with a high charge density is more easily  
2 intercalated in the interlayer of Mg-Al LDH than an anion with a low charge density.<sup>9,10</sup>  
3 However, the principles involved in the removal of organic anions by Mg-Al LDH and  
4 Mg-Al oxide are unknown. It is unclear whether an organic anion with a high charge  
5 density is more easily intercalated in the interlayer of Mg-Al LDH than an organic anion  
6 with a low charge density, as well as than an inorganic anion. Different factors may affect  
7 the intercalation of organic anions in the interlayer of Mg-Al LDH. On the other hand,  
8 Mg-Al LDHs intercalated with dodecylsulfate ( $DS^-$ ), 2-naphthalenesulfonate ( $NS^-$ ), and  
9 2,6-naphthalene disulfonate ( $2,6-NDS^{2-}$ ) were found to show an uptake capacity for  
10 bisphenol A in an aqueous solution, probably because of the hydrophobic interactions  
11 between the benzene rings of bisphenol A and the aromatic anion intercalated in the  
12 interlayer.<sup>11,12</sup> The uptake of bisphenol A was not based on the anion-uptake property of  
13 Mg-Al LDH and Mg-Al oxide, because bisphenol A is nonionic. We have clarified that  
14 Mg-Al LDH modified with an organic anion could take up nonionic organic substances  
15 owing to hydrophobic interactions.<sup>11,12</sup> Such hydrophobic interactions are predicted to  
16 affect the removal of organic anions by Mg-Al LDH and Mg-Al oxide. In this study, this  
17 hypothesis was examined for the reconstruction of Mg-Al LDH from Mg-Al oxide. In  
18 particular, the removal of aromatic sulfonates such as benzenesulfonate ( $BS^-$ ) and  $NS^-$  by

1 the Mg-Al oxide from aqueous solution was investigated for studying the equilibrium and  
2 kinetics involved in the removal process. Figure 1 shows the molecular structures of  $\text{BS}^-$   
3 and  $\text{NS}^-$ ; the molecular geometry of the isolated  $\text{BS}^-$  and  $\text{NS}^-$  in the ground state was  
4 calculated at the Hartree-Fock/STO-3G level of theory with Gaussian 03.<sup>13</sup> The  
5 molecular lengths increase in the order of  $\text{BS}^- < \text{NS}^-$ , but the charge density decreases in  
6 the order of  $\text{BS}^- > \text{NS}^-$ . The effects of the hydrophobic interactions and charge density of  
7 the anion on the removal of  $\text{BS}^-$  and  $\text{NS}^-$  by the Mg-Al oxide were also investigated.

8

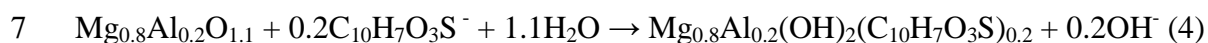
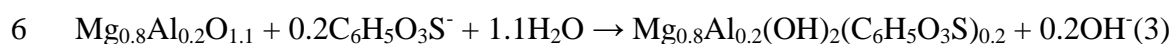
9

## 10 **Experimental**

11 All chemicals were reagent grade and used without further purification. The  
12 Mg-Al oxide was obtained by the thermal decomposition of Mg-Al LDH intercalated  
13 with  $\text{CO}_3^{2-}$  ( $\text{CO}_3\cdot\text{Mg-Al}$  LDH), which was prepared using the method described in our  
14 previous paper.<sup>14</sup> The Mg-Al oxide contained 39.3 wt% Mg and 10.7 wt% Al, with the  
15 Mg/Al molar ratio being 4.1. We prepared  $\text{BS}^-$  and  $\text{NS}^-$  solutions by dissolving  
16  $\text{C}_6\text{H}_5\text{NaO}_3\text{S}$  and  $\text{C}_{10}\text{H}_7\text{NaO}_3\text{S}$  in deionized water, respectively. The Mg-Al oxide was  
17 added to 2 mmol/L  $\text{BS}^-$  or  $\text{NS}^-$  solutions (500 mL), and the resultant suspensions were  
18 stirred at 10–60 °C for 1440 min.  $\text{N}_2$  was bubbled through the solutions throughout the



1 procedure, and pH was continuously measured during the reaction. Samples of the  
2 suspensions were withdrawn at different time intervals and immediately filtered through  
3 a 0.45- $\mu\text{m}$  membrane filter. The filtrates were analyzed for residual  $\text{BS}^-$  or  $\text{NS}^-$ . The Mg–  
4 Al oxide was used in stoichiometric quantity for  $\text{BS}^-$  or  $\text{NS}^-$  removal, as shown in  
5 Equations (3) and (4):



8 To determine the adsorption isotherm of  $\text{BS}^-$  or  $\text{NS}^-$  adsorbed by the Mg–Al  
9 oxide,  $\text{BS}^-$  or  $\text{NS}^-$  solution (50 mL, 1–15 mM) and Mg–Al oxide (0.1 g) were placed in  
10 100-mL screw-top tubes and shaken at 10–60 °C for 1440 min.

11 The materials were analyzed using XRD with Cu  $\text{K}\alpha$  radiation. For the  
12 adsorption experiments, the residual concentrations of  $\text{BS}^-$  or  $\text{NS}^-$  in the filtrates were  
13 determined using HPLC.

14

15

## 16 Results and Discussion

### 17 *Kinetics and equilibrium studies of the removal of aromatic sulfonates*

18 Figures 2 and 3 show the effect of temperature on the degree of  $\text{BS}^-$  and  $\text{NS}^-$  removal by

1 the suspension of Mg–Al oxide in the BS<sup>-</sup> and NS<sup>-</sup> solutions. In both the adsorbates, the  
2 removal increased with time at all temperatures. The Mg–Al oxide was confirmed to take  
3 up BS<sup>-</sup> and NS<sup>-</sup> in aqueous solution according to Equations (3) and (4). For BS<sup>-</sup>, the  
4 removal rate increased with the temperature at any given time. For NS<sup>-</sup>, the removal rate  
5 increased with the temperature within 120 min of beginning the process. Figures 4 and 5  
6 show the effect of temperature on pH variation during BS<sup>-</sup> or NS<sup>-</sup> removal by the  
7 suspension of the Mg–Al oxide in the BS<sup>-</sup> or NS<sup>-</sup> solution. At all temperatures, the pH  
8 increased rapidly with time, until it attained the pH of 10–12 and remained constant. This  
9 increase in the pH values is attributed to the release of OH<sup>-</sup>, as shown in Equations (3) and  
10 (4). The accelerated rate of BS<sup>-</sup> or NS<sup>-</sup> removal at higher temperatures in the initial  
11 reaction stage implies that the reaction proceeds under chemical reaction control.  
12 Therefore, the kinetics of BS<sup>-</sup> or NS<sup>-</sup> removal by the Mg–Al oxide was examined until 60  
13 min in order to check the initial reaction rate. First-order kinetics, which depends on the  
14 concentration of BS<sup>-</sup> or NS<sup>-</sup>, can be expressed as follows:

$$15 \quad -\ln(1 - x) = kt, \quad (5)$$

16 where  $x$  is the degree of BS<sup>-</sup> or NS<sup>-</sup> removal,  $t$  (min) is the reaction time, and  $k$  (min<sup>-1</sup>) is  
17 the rate constant for BS<sup>-</sup> or NS<sup>-</sup> removal. Figures 6 and 7 show the pseudo-first-order plot  
18 of BS<sup>-</sup> or NS<sup>-</sup> removal by the suspension of Mg–Al oxide in BS<sup>-</sup> or NS<sup>-</sup> solution. In both

1 cases, a good linearity was obtained at all temperatures, indicating that  $\text{BS}^-$  or  $\text{NS}^-$   
2 removal can be represented by pseudo-first-order reaction kinetics. For  $\text{BS}^-$ , the apparent  
3 rate constants at 10, 30, and 60 °C were found to be  $4.7 \times 10^{-3}$ ,  $1.4 \times 10^{-2}$ , and  $1.0 \times 10^{-1}$   
4  $\text{min}^{-1}$ , respectively; for  $\text{NS}^-$ , the corresponding values were  $6.0 \times 10^{-3}$ ,  $2.2 \times 10^{-2}$ , and  $8.8$   
5  $\times 10^{-2} \text{ min}^{-1}$ , respectively. Thus, the apparent rate constants clearly increased with  
6 temperature. An Arrhenius plot of the rate constants (Figure 8) yields an apparent  
7 activation energy of 48 and 42  $\text{kJ mol}^{-1}$  for  $\text{BS}^-$  and  $\text{NS}^-$  removal, respectively. These  
8 values confirm that  $\text{BS}^-$  or  $\text{NS}^-$  removal by the Mg–Al oxide proceeded under chemical  
9 reaction control. This chemical reaction involves the adsorption of  $\text{BS}^-$  or  $\text{NS}^-$  by the  
10 Mg–Al oxide according to Equations (3) and (4).

11 Table 1 shows the equilibrium concentration, pH, and relative distribution ratio  
12 ( $K$ ) values after the formation of the Mg–Al oxide suspension in the  $\text{BS}^-$  or  $\text{NS}^-$  solution.  
13 In particular,  $K$  for the removal of  $\text{OH}^-$  and  $\text{BS}^-$  or  $\text{NS}^-$  by the Mg–Al oxide is defined as  
14 follows:

$$15 \quad K = K_{\text{d,A}}/K_{\text{d,OH}} \quad [K_{\text{d,A}} = m_{\text{A}}(\text{Solid})/m_{\text{A}}(\text{Soln.}), K_{\text{d,OH}} = m_{\text{OH}}(\text{Solid})/m_{\text{OH}}(\text{Soln.})] \quad (6)$$

16 In this case,  $m_{\text{A}}(\text{Solid})$  and  $m_{\text{A}}(\text{Soln.})$  indicate the amount of  $\text{BS}^-$  or  $\text{NS}^-$  in solid and  
17 solution, respectively; and  $m_{\text{OH}}(\text{Solid})$  and  $m_{\text{OH}}(\text{Soln.})$  represent the amount of  $\text{OH}^-$  in  
18 solid and solution, respectively.  $K$  values followed the order:  $\text{NS}^- > \text{BS}^-$ . The Mg–Al

1 oxide was found to take up  $\text{NS}^-$  more preferentially than  $\text{BS}^-$ . However, the  $K$  values for  
2  $\text{BS}^-$  and  $\text{NS}^-$  were lower than 1, suggesting that the Mg–Al oxide took up  $\text{OH}^-$  more  
3 preferentially than  $\text{BS}^-$  and  $\text{NS}^-$ . Thus, the  $K$  values followed the order:  $\text{OH}^- > \text{NS}^- > \text{BS}^-$ .  
4  $\text{OH}^-$  is produced by the rehydration of the Mg–Al oxide, according to Equations (3) and  
5 (4). This is supported by the fact that the solution pH values increase (Figures 4 and 5). As  
6 shown in Figures 2 and 3, the Mg–Al oxide cannot take up large amounts of  $\text{BS}^-$  and  $\text{NS}^-$   
7 from aqueous solution at the stoichiometric quantity. This is because of the intercalation  
8 of the produced  $\text{OH}^-$  in the interlayer of Mg–Al LDH according to Equation (7).



10 Figures 9 and 10 show the adsorption isotherms for the adsorption of  $\text{BS}^-$  or  $\text{NS}^-$   
11 by the Mg–Al oxide. In both the adsorbates, the equilibrium-adsorption amount increased  
12 proportionally with the equilibrium concentration at all temperatures. The adsorption  
13 isotherms did not follow adsorption models such as Halsey and Henderson models;  
14 instead, they appeared a Langmuir-type behavior, as confirmed by using the experimental  
15 data in the Langmuir equation shown below:

$$16 \quad q_e = C_e q_m K_L / (1 + C_e K_L), \quad (8)$$

1 where  $q_e$  ( $\text{mmol g}^{-1}$ ) is the equilibrium adsorption,  $C_e$  (mM) is the equilibrium  
2 concentration,  $q_m$  ( $\text{mmol g}^{-1}$ ) is the maximum adsorption, and  $K_L$  is the equilibrium  
3 adsorption constant. This equation can also be expressed as:

$$4 \quad C_e/q_e = 1/q_m K_L + C_e/q_m. \quad (9)$$

5 Figures 11 and 12 show a plot of  $C_e/q_e$  versus  $C_e$  of the adsorption isotherms for the  
6 adsorption of  $\text{BS}^-$  or  $\text{NS}^-$  by the Mg–Al oxide. In all cases, a good linearity was obtained,  
7 confirming that this process follows a Langmuir-type adsorption. Table 2 lists the values  
8 of  $q_m$  and  $K_L$  of  $\text{BS}^-$  and  $\text{NS}^-$  adsorbed by the Mg–Al oxide, as determined from the slope  
9 and intercept of the linear fit of the data given in Figures 11 and 12. At all temperatures,  
10 the maximum and equilibrium adsorption constants for  $\text{NS}^-$  were larger than those for  
11  $\text{BS}^-$ . These results also indicate that the Mg–Al oxide can take up  $\text{NS}^-$  more easily than  
12  $\text{BS}^-$ .

13 The results of the kinetics and equilibrium studies clearly suggest that the  
14 Mg–Al oxide can be more easily combined with  $\text{NS}^-$  than with  $\text{BS}^-$ , i.e., the Mg–Al oxide  
15 reacts more favorably with aromatic sulfonates with lower charge density, unlike in the  
16 removal of inorganic anions. The effect of hydrophobic interactions is larger than that of  
17 electrostatic interactions in the removal of aromatic sulfonates by the Mg–Al oxide.  
18 Usually, inorganic anion removal by the Mg–Al oxide is promoted by electrostatic

1 interactions, and the order of the inorganic anion removal is controlled by its charge  
2 density. It is known that the aromatic rings of two aromatic sulfonates interact via  
3 hydrophobic interactions in aqueous solution. The hydrophobic interactions of  $\text{NS}^-$   
4 molecules are stronger than those of the  $\text{BS}^-$  molecules, because  $\text{NS}^-$  has a naphthalene  
5 ring in its structure and  $\text{BS}^-$  has a benzene ring. In contrast, the electrostatic interactions  
6 of  $\text{NS}^-$  are typically weaker than those of  $\text{BS}^-$ , because its charge density is lower than that  
7 of  $\text{BS}^-$ . In the initial reaction stage, the Mg-Al oxide rehydrates and combines with  
8 aromatic sulfonate to reconstruct the LDH structure. Then, the aromatic sulfonate  
9 intercalated in the interlayer of the reconstructed Mg-Al LDH attracts the aromatic  
10 sulfonate in aqueous solution via hydrophobic interactions, which may promote the  
11 removal of the aromatic sulfonate by the Mg-Al oxide. Because the attraction of  $\text{NS}^-$   
12 molecules is stronger than that of  $\text{BS}^-$  molecules, the removal of  $\text{NS}^-$  by the Mg-Al oxide  
13 is more efficient than that of  $\text{BS}^-$ . Notably, the removal of the aromatic sulfonate by the  
14 Mg-Al oxide is controlled by hydrophobic interactions.

#### 15 *Molecular orientation of aromatic sulfonates in the interlayer of Mg-Al LDH*

16 Figures 13 and 14 show the XRD patterns of the products obtained by the  
17 suspension of Mg-Al oxide in  $\text{BS}^-$  and  $\text{NS}^-$  solutions at 30 °C. The XRD peaks for all the  
18 products can be assigned to hydrotalcite (JCPDS card 22-700), indicating that the LDH

1 structure was formed after the removal of  $\text{BS}^-$  and  $\text{NS}^-$ . This confirms the reconstruction  
2 of Mg–Al LDH from the Mg–Al oxide with the intercalation of  $\text{BS}^-$  and  $\text{NS}^-$ , as shown in  
3 Equations (3) and (4). Because the XRD peaks of LDH are generally indexed on the basis  
4 of a hexagonal unit cell, the basal spacing of LDH is equivalent to  $1/n^{\text{th}}$  of the  $c$  parameter,  
5 where  $n$  is the number of the layer repeat of the unit cell.<sup>15</sup> The basal spacing consists of  
6 an Al-bearing brucite-like octahedral layer, whose thickness and interlayer spacing are  
7 affected by the size and orientation of the interlayer anion. Based on the XRD patterns,  
8 basal spacing  $d_{003}$  in the product ( $Ce = 0.5 \text{ mmol L}^{-1}$ ) obtained by the suspension of  
9 Mg–Al oxide in  $\text{BS}^-$  solution was calculated to be  $8.1 \text{ \AA}$  (Figure 13(a)). Assuming a  
10 brucite-like layer thickness of approximately  $4.8 \text{ \AA}$ , as reported by Miyata,<sup>16</sup> the  
11 interlayer spacing is calculated to be  $3.3 \text{ \AA}$ . In this case, the molecular structures of  $\text{BS}^-$   
12 and  $\text{NS}^-$  contain a planar-structured aromatic ring, and the molecular size in the direction  
13 perpendicular to the planar structure is determined by the size of the  $-\text{SO}_3^-$  group. As  
14 reported in our previous study, the molecular size in this direction is  $3.1 \text{ \AA}$ .<sup>17</sup> This is very  
15 close to the interlayer spacing of  $3.3 \text{ \AA}$  for the product with  $Ce = 0.5 \text{ mmol L}^{-1}$ . Therefore,  
16 the benzene ring of  $\text{BS}^-$  may be oriented parallel to the brucite-like host layers of Mg–Al  
17 LDH (Figure 15(a)); basal spacing  $d_{003}$  in the product (for  $Ce = 2.8\text{--}9.5 \text{ mmol L}^{-1}$ ) was  
18 found to be around  $9 \text{ \AA}$  (Figures 13(b)–(d)), and the interlayer spacing is calculated to be

1 4.2 Å, which expands from that of the product (for  $C_e = 0.5 \text{ mmol L}^{-1}$ ). As shown in  
2 Figure 9 and 13, the equilibrium adsorption amounts and the XRD patterns for  $C_e = 2.8\text{--}$   
3  $9.5 \text{ mmol L}^{-1}$  were almost similar. This suggests the benzene rings of  $\text{BS}^-$  have a similar  
4 orientation in the interlayer of Mg-Al LDH. The interlayer spacing is larger than the  
5 molecular size in the direction perpendicular to the planar structure, as determined by the  
6 size of the  $\text{-SO}_3^-$  group. Therefore, the two benzene rings of  $\text{BS}^-$  may overlap in the  
7 brucite-like host layers of Mg-Al LDH (Figure 15(b)). Because the XRD peak at a  $2\theta$   
8 value of  $22^\circ$  was observed for the products for  $C_e = 2.8\text{--}9.5 \text{ mmol L}^{-1}$  as well as for  $C_e =$   
9  $0.5 \text{ mmol L}^{-1}$  (Figure 13), the orientation of the benzene ring of  $\text{BS}^-$  (Figure 15(a)) is  
10 considered to be also remained for the products for  $C_e = 2.8\text{--}9.5 \text{ mmol L}^{-1}$ . Because of  
11 their weaker hydrophobic attractions, the  $\text{BS}^-$  molecules cannot be fully accommodated  
12 in the interlayer of Mg-Al LDH (such as in the case of perpendicular orientation).  
13 However, data in Figures 13(b)–(d) support the presence of hydrophobic interactions  
14 between the benzene rings of  $\text{BS}^-$  in the interlayer of Mg-Al LDH.

15 In addition, basal spacing  $d_{003}$  in the product ( $C_e = 0.03 \text{ mmol L}^{-1}$ ), which was  
16 obtained by the suspension of Mg–Al oxide in the  $\text{NS}^-$  solution, was found to be 8.3 Å  
17 (Figure 14(a)), and the interlayer spacing was calculated to be 3.5 Å. This is very close to  
18 the molecular size in the direction perpendicular to the planar-structured naphthalene ring

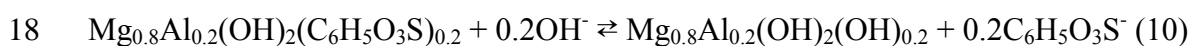


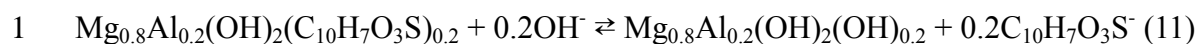
1 as determined by the size of the  $-\text{SO}_3^-$  group. This indicates that the naphthalene ring of  
2  $\text{NS}^-$  may be oriented along an arrangement that is parallel to the brucite-like host layers of  
3 Mg-Al LDH (Figure 16(a)). Figure 14(b) displays the expansion of basal spacing  $d_{003}$   
4 from 8.3 to 9.0 Å. As shown in Figure 10, the equilibrium adsorption amount increased as  
5  $C_e$  increased from 0.03 to 1.1  $\text{mmol L}^{-1}$ . Because the XRD shoulder peak is also observed  
6 at a  $2\theta$  value of  $5^\circ$  (Figure 14(b)), the orientation of the naphthalene ring of  $\text{NS}^-$  is  
7 probably different from that shown in Figure 16(a). Figures 14(c) and (d) show spacings  
8  $d_{003}$  and  $d_{006}$  of around 19 and 9 Å, respectively, which indicate an interlayer spacing of  
9 around 14 Å. This value is larger than the molecular size (9.16 Å) of  $\text{NS}^-$  (Figure 1(b)).  
10 Therefore, the naphthalene ring of  $\text{NS}^-$  may be oriented along an arrangement that is  
11 perpendicular to the brucite-like host layers of Mg-Al LDH (Figure 16(b)). This  
12 phenomenon has also been reported in our previous paper.<sup>17-19</sup> In particular, the XRD  
13 patterns for the  $\text{NS}^-$ -intercalated Mg-Al LDH prepared by co-precipitation<sup>18</sup> are similar  
14 to those for the products obtained by the suspension of the Mg-Al oxide in  $\text{NS}^-$  solution.  
15 Data in Figure 14(b) also suggest the presence of the perpendicular orientation. Because  
16 of their stronger hydrophobic attraction,  $\text{NS}^-$  molecules can be effectively accommodated  
17 in the interlayer of Mg-Al LDH in a perpendicular orientation. Figures 14(b)–(d) confirm  
18 the presence of hydrophobic interactions between the benzene rings of  $\text{NS}^-$  in the

1 interlayer of Mg-Al LDH.

2 *Effect of temperature at longer time durations*

3 Table 2 shows that the maximum and equilibrium adsorption constants decrease  
 4 when the temperature is increased from 30 to 60 °C for both BS<sup>-</sup> and NS<sup>-</sup>. Table 3 shows  
 5 the amount of BS<sup>-</sup> and NS<sup>-</sup> removed by the Mg–Al oxide at 1440 min. At 60 °C, the BS<sup>-</sup>  
 6 removal was determined to be 44.5% at 180 min (Figure 2), decreasing to 12.9% at 1440  
 7 min. At the same temperature, the NS<sup>-</sup> removal was found to be 38.8% at 240 min (Figure  
 8 3), decreasing to 23.3% at 1440 min. At 1440 min, while the amounts of BS<sup>-</sup> and NS<sup>-</sup>  
 9 removed decreased at 60 °C, they were almost constant at 10 and 30 °C. Table 4 shows the  
 10 change in the pH value on BS<sup>-</sup> and NS<sup>-</sup> removal by the Mg–Al oxide at 1440 min. For  
 11 both adsorbates, the pH values at 10 and 30 °C were almost constant from the last points  
 12 shown in Figures 4 and 5 to 1440 min. However, at 60 °C, the pH value on BS<sup>-</sup> removal  
 13 was determined to be 10.7 at 180 min (Figure 4), decreasing to 10.4 at 1440 min. At the  
 14 same temperature, the pH value on NS<sup>-</sup> removal was found to be 10.4 at 240 min (Figure  
 15 5), decreasing to 10.2 at 1440 min. These results suggest that OH<sup>-</sup> was anion-exchanged  
 16 with BS<sup>-</sup> and NS<sup>-</sup> intercalated in the Mg-Al LDH interlayer at 60 °C, as shown in  
 17 Equations. (10) and (11).





2 Although the removal of  $\text{BS}^-$  and  $\text{NS}^-$  by Mg–Al oxide was promoted in the initial  
3 reaction stage at 60 °C, the intercalation of  $\text{OH}^-$  was probably promoted in the second  
4 reaction stage owing to the increased activity of  $\text{OH}^-$  at 60 °C. This is in agreement with  
5 the findings discussed above that  $K$  follows the order  $\text{OH}^- > \text{NS}^- > \text{BS}^-$ . In the case of the  
6 lower  $\text{OH}^-$  activity at 10 and 30 °C, the anion exchange of the intercalated  $\text{BS}^-$  and  $\text{NS}^-$   
7 with  $\text{OH}^-$  is not promoted in the second reaction stage.

8

9

## 10 **Conclusions**

11 Data presented in this work confirmed that Mg–Al oxide can take up  
12 benzenesulfonate ( $\text{BS}^-$ ) and 2-naphthalenesulfonate ( $\text{NS}^-$ ) from aqueous solution, and that  
13 the removal can be described by pseudo-first-order reaction kinetics.  $\text{BS}^-$  or  $\text{NS}^-$  removal  
14 by Mg–Al oxide proceeds under chemical reaction control. Interestingly, our data showed  
15 that the Mg–Al oxide preferentially takes up  $\text{OH}^-$  over  $\text{BS}^-$  and  $\text{NS}^-$ , with relative  
16 distribution ratio ( $K$ ) following the order:  $\text{OH}^- > \text{NS}^- > \text{BS}^-$ . This process follows a  
17 Langmuir-type adsorption, and the maximum and equilibrium adsorption constant for  
18  $\text{NS}^-$  were larger than those for  $\text{BS}^-$ , confirming that the Mg–Al oxide reacts more

1 favorably with  $\text{NS}^-$  than with  $\text{BS}^-$ . The fact that Mg-Al oxide preferentially reacts with  
2 aromatic sulfonates with lower charge density is in contrast to the trend observed for the  
3 removal of inorganic anions. For the removal of aromatic sulfonates, the effect of the  
4 hydrophobic interactions is larger than that of electrostatic interactions. Although the  
5 order of the inorganic anion removal is controlled by the charge density, the removal of  
6 aromatic sulfonates by the Mg-Al oxide was found to be controlled by hydrophobic  
7 interactions. In the initial reaction stage, the Mg-Al oxide rehydrates and combines with  
8 the aromatic sulfonate to reconstruct the layered double hydroxide (LDH) structure.  
9 Then, the aromatic sulfonate, intercalated in the interlayer of the reconstructed Mg-Al  
10 LDH, interacts with the aromatic sulfonates via hydrophobic interactions, which  
11 facilitates their removal. Because the attraction of  $\text{NS}^-$  molecules is stronger than that of  
12  $\text{BS}^-$  molecules, the removal of  $\text{NS}^-$  by the Mg-Al oxide was found to be more efficient.  
13 For  $\text{BS}^-$ , the benzene ring is possibly oriented along an arrangement that is parallel to the  
14 brucite-like host layers of Mg-Al LDH in the case of a low equilibrium concentration  
15 ( $C_e$ ). With increasing  $C_e$ , the two benzene rings may overlap. For  $\text{NS}^-$ , the naphthalene  
16 ring may be oriented along an arrangement that is parallel to the brucite-like host layers of  
17 Mg-Al LDH in the case of a low  $C_e$ . With increasing  $C_e$ , the naphthalene ring of  $\text{NS}^-$  is  
18 possibly oriented along an arrangement that is perpendicular to the brucite-like host

1 layers of Mg-Al LDH.

2

**1 Notes and references**

- 2 1 F. Cavani, F. Trifirò, A. Vaccari, *Catal. Today* 1991, **11**, 173.
- 3 2 L. Ingram, H.F.W. Taylor, *Mineral. Mag.* 1967, **36**, 465.
- 4 3 R. Allmann, *Acta Crystallogr.* 1968, **B24**, 972.
- 5 4 S.J. Mills, A.G. Christy, J.-M.R. Génin, T. Kameda, F. Colombo, *Mineral. Mag.* 2012,
- 6 **76**, 1289.
- 7 5 R. Extremera, I. Pavlovic, M.R. Pérez, C. Barriga, *Chem. Eng. J.* 2012, **213**, 392.
- 8 6 A.R. Auxillio, P.C. Andrews, P.C. Junk, L. Spiccia, *Dyes Pigments* 2009, **81**, 103.
- 9 7 E. Geraud, M. Bouhent, Z. Derriche, F. Leroux, V. Prévot, C. Forano, *J. Phys. Chem.*
- 10 *Solids*, 2007, **68**, 818.
- 11 8 W. Tsai, C. Chang, M. Lin, S. Chien, H. Sun, M. Hsieh, *Chemosphere*, 2001, **45**, 51.
- 12 9 S. Miyata, *Clays Clay Miner.* 1983, **31**, 305.
- 13 10 T. Kameda, F. Yabuuchi, T. Yoshioka, M. Uchida, A. Okuwaki, *Water Res.* 2003, **37**,
- 14 1545.
- 15 11 T. Kameda, M. Saito, Y. Umetsu, *J. Alloys Comp.* 2005, **402**, 46.
- 16 12 T. Kameda, M. Saito, Y. Umetsu, *Mater. Trans.* 2007, 48, 2225.
- 17 13 Gaussian 03, Revision 3.09, M.J. Frisch, G.W. Trucks, H.B. Schlegel, G.E. Scuseria,
- 18 M.A. Robb, J.R. Cheeseman, J.A. Montgomery Jr., T. Vreven, K.N. Kudin, J.C.

- 1 Burant, J.M. Millam, S.S. Iyengar, J. Tomasi, V. Barone, B. Mennucci, M. Cossi, G.  
2 Scalmani, N. Rega, G.A. Petersson, H. Nakatsuji, M. Hada, M. Ehara, K. Toyota, R.  
3 Fukuda, J. Hasegawa, M. Ishida, T. Nakajima, Y. Honda, O. Kitao, H. Nakai, M.  
4 Klene, X. Li, J.E. Knox, H.P. Hratchian, J.B. Cross, V. Bakken, C. Adamo, J.  
5 Jaramillo, R. Gomperts, R.E. Stratmann, O. Yazyev, A.J. Austin, R. Cammi, C.  
6 Pomelli, J.W. Ochterski, P.Y. Ayala, K. Morokuma, G.A. Voth, P. Salvador, J.J.  
7 Dannenberg, V.G. Zakrzewski, S. Dapprich, A.D. Daniels, M.C. Strain, O. Farkas,  
8 D.K. Malick, A.D. Rabuck, K. Raghavachari, J.B. Foresman, J.V. Ortiz, Q. Cui, A.G.  
9 Baboul, S. Clifford, J. Cioslowski, B.B. Stefanov, G. Liu, A. Liashenko, P. Piskorz, I.  
10 Komaromi, R.L. Martin, D.J. Fox, T. Keith, M.A. Al-Laham, C.Y. Peng, A.  
11 Nanayakkara, M. Challacombe, P.M.W. Gill, B. Johnson, W. Chen, M.W. Wong, C.  
12 Gonzalez, J.A. Pople, Gaussian, Inc., Wallingford, CT, 2004.
- 13 14 T. Kameda, M. Honda, T. Yoshioka: *Sep. Purif. Technol.* 2011, **80**, 235.
- 14 15 S.P. Newman, W. Jones: *New J. Chem.* 1998, **22**, 105.
- 15 16 S. Miyata: *Clays Clay Miner.* 1975, **23**, 369.
- 16 17 T. Kameda, Y. Tsuchiya, T. Yamazaki, T. Yoshioka: *Solid State Sci.* 2009, **11**, 2060.
- 17 18 T. Kameda, M. Saito, Y. Umetsu: *Mater. Trans.* 2006, **47**, 923.
- 18 19 T. Kameda, T. Yamazaki, T. Yoshioka: *Micro. Meso. Mater.* 2008, **114**, 410.

1

2

3

4



1 **Figure legends**

2 Fig. 1. Molecular structure of (a)  $\text{BS}^-$  and (b)  $\text{NS}^-$ .

3

4 Fig. 2. Effect of temperature on the degree of  $\text{BS}^-$  removal by the suspension of the  
5 Mg–Al oxide in  $\text{BS}^-$  solution.

6

7 Fig. 3. Effect of temperature on the degree of  $\text{NS}^-$  removal by the suspension of the  
8 Mg–Al oxide in  $\text{NS}^-$  solution.

9

10 Fig. 4. Effect of temperature on pH variation during  $\text{BS}^-$  removal by the suspension of the  
11 Mg–Al oxide in  $\text{BS}^-$  solution.

12

13 Fig. 5. Effect of temperature on pH variation during  $\text{NS}^-$  removal by the suspension of the  
14 Mg–Al oxide in  $\text{NS}^-$  solution.

15

16 Fig. 6. Pseudo-first-order plot of  $\text{BS}^-$  removal by the suspension of the Mg–Al oxide in  
17  $\text{BS}^-$  solution.

18

1 Fig. 7. Pseudo-first-order plot of  $\text{NS}^-$  removal by the suspension of the Mg–Al oxide in  
2  $\text{NS}^-$  solution.

3

4 Fig. 8. Arrhenius plot of the apparent rate constant of  $\text{BS}^-$  and  $\text{NS}^-$  removal by the  
5 suspension of the Mg–Al oxide in  $\text{BS}^-$  and  $\text{NS}^-$  solutions.

6

7 Fig. 9. Adsorption isotherm of  $\text{BS}^-$  adsorbed by the Mg–Al oxide for 1440 min.

8

9 Fig. 10. Adsorption isotherm of  $\text{NS}^-$  adsorbed by the Mg–Al oxide for 1440 min.

10

11 Fig. 11.  $C_e$  versus  $C_e/q_e$  plots for the adsorption isotherm of  $\text{BS}^-$  adsorbed by the Mg–Al  
12 oxide.

13

14 Fig. 12.  $C_e$  versus  $C_e/q_e$  plots for the adsorption isotherm of  $\text{NS}^-$  adsorbed by the Mg–Al  
15 oxide.

16

1 Fig. 13. XRD patterns for the products obtained by the suspension of the Mg–Al oxide in  
2  $\text{BS}^-$  solution at 30 °C; (a)  $C_e = 0.5 \text{ mmol L}^{-1}$ , (b)  $C_e = 2.8 \text{ mmol L}^{-1}$ , (c)  $C_e = 5.0 \text{ mmol}$   
3  $\text{L}^{-1}$ , (d)  $C_e = 9.5 \text{ mmol L}^{-1}$ .

4

5 Fig. 14. XRD patterns for the products obtained by the suspension of the Mg–Al oxide in  
6  $\text{NS}^-$  solution at 30 °C; (a)  $C_e = 0.03 \text{ mmol L}^{-1}$ , (b)  $C_e = 1.1 \text{ mmol L}^{-1}$ , (c)  $C_e = 2.9 \text{ mmol}$   
7  $\text{L}^{-1}$ , (d)  $C_e = 7.7 \text{ mmol L}^{-1}$ .

8

9 Fig. 15. Proposed molecular orientation of  $\text{BS}^-$  intercalated in the interlayer of Mg–Al  
10 LDH; (a)  $C_e = 0.5 \text{ mmol L}^{-1}$ , (b)  $C_e = 2.8\text{--}9.5 \text{ mmol L}^{-1}$ .

11

12 Fig. 16. Proposed molecular orientation of  $\text{NS}^-$  intercalated in the interlayer of Mg–Al  
13 LDH. (a)  $C_e = 0.03 \text{ mmol L}^{-1}$ , (b)  $C_e = 2.9\text{--}7.7 \text{ mmol L}^{-1}$ .

14

15

## 16 Table captions

17 Table 1. Equilibrium concentration and pH and relative distribution ratio ( $K$ ) after the  
18 suspension of the Mg–Al oxide in  $\text{BS}^-$  or  $\text{NS}^-$  solution.

1

2 Table 2. Values of  $q_m$  and  $K_L$  on  $BS^-$  and  $NS^-$  adsorbed by the Mg–Al oxide.

3

4 Table 3.  $BS^-$  and  $NS^-$  removal by the Mg–Al oxide at 1440 min.

5

6 Table 4. pH value on  $BS^-$  and  $NS^-$  removal by the Mg–Al oxide at 1440 min.

7

8

9

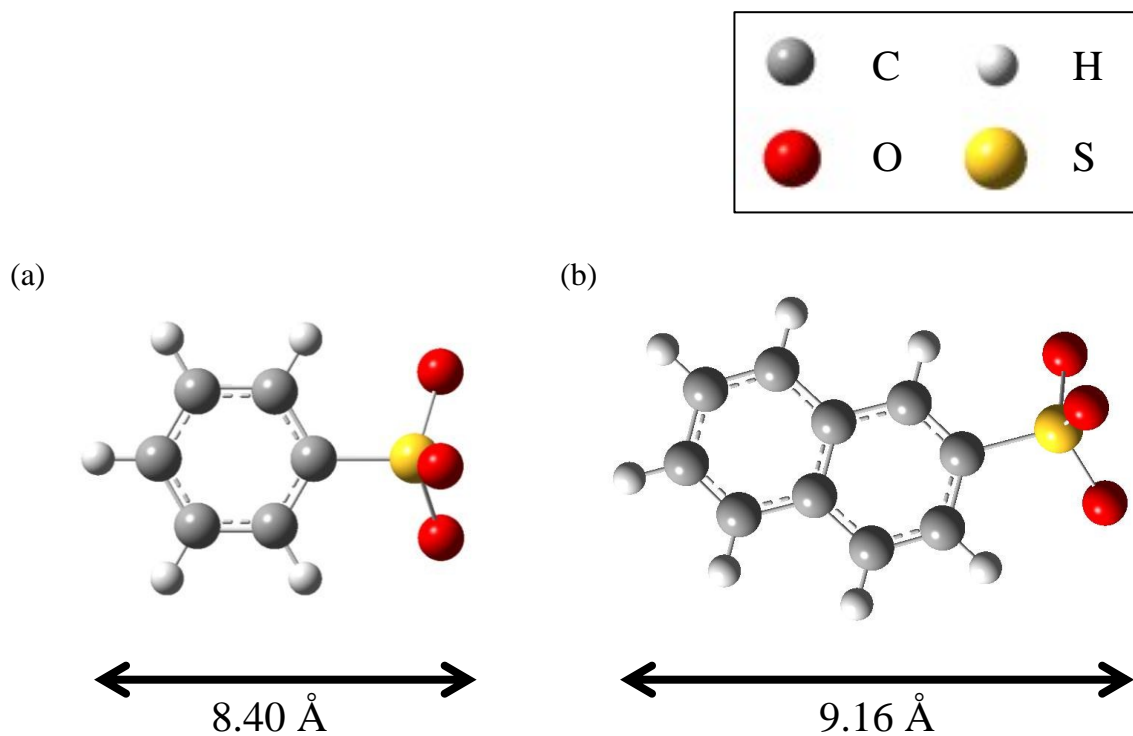


Fig. 1. Molecular structure of (a)  $\text{BS}^-$  and (b)  $\text{NS}^-$ .

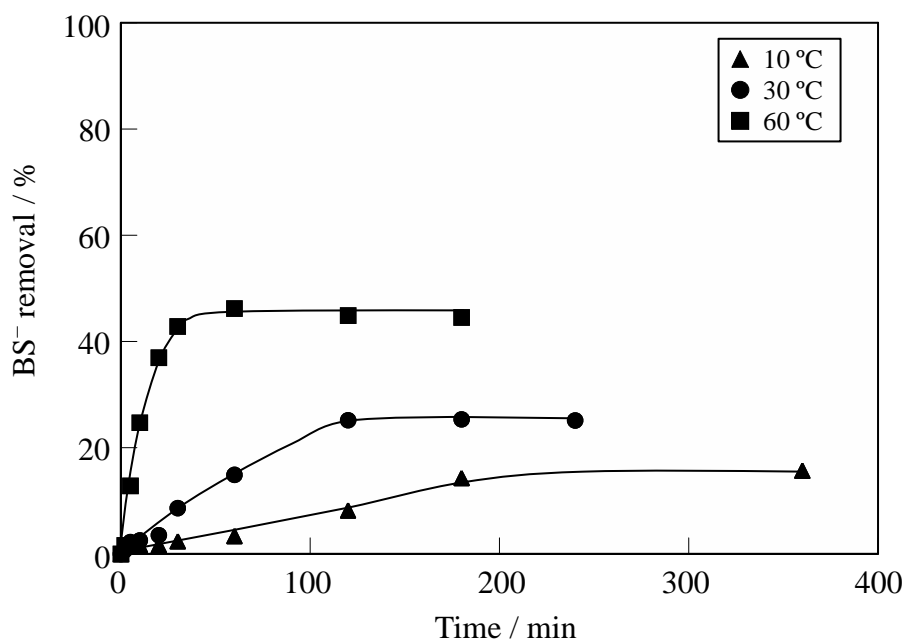


Fig. 2. Effect of temperature on the degree of  $\text{BS}^-$  removal by the suspension of the Mg–Al oxide in  $\text{BS}^-$  solution.

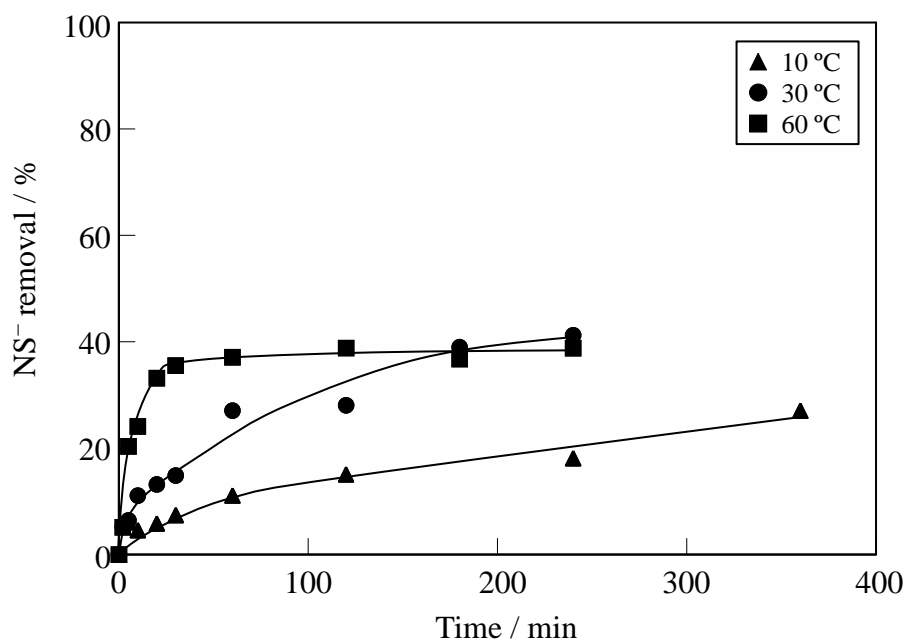


Fig. 3. Effect of temperature on the degree of NS<sup>-</sup> removal by the suspension of the Mg–Al oxide in NS<sup>-</sup> solution.

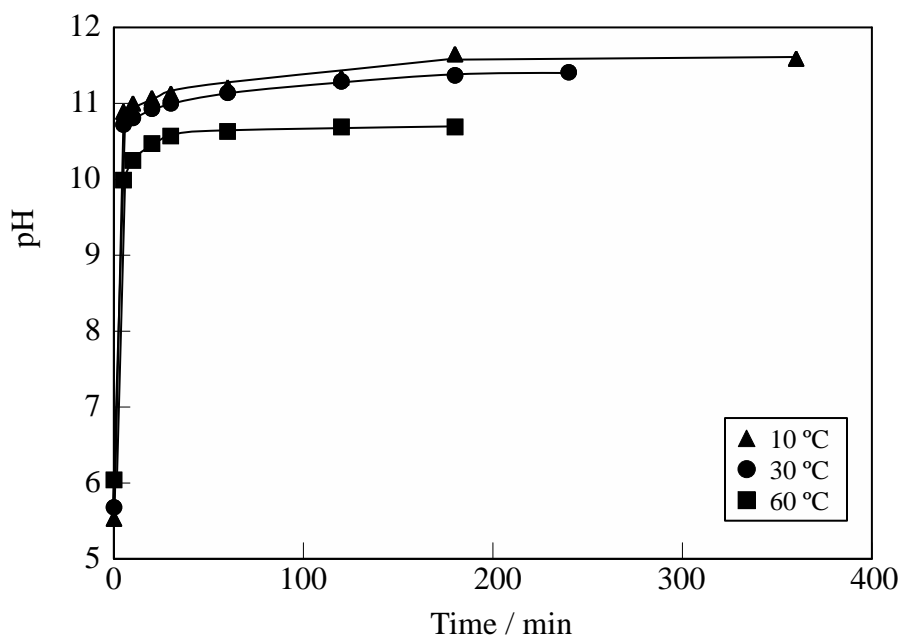


Fig. 4. Effect of temperature on pH variation during  $\text{BS}^-$  removal by the suspension of the Mg–Al oxide in  $\text{BS}^-$  solution.



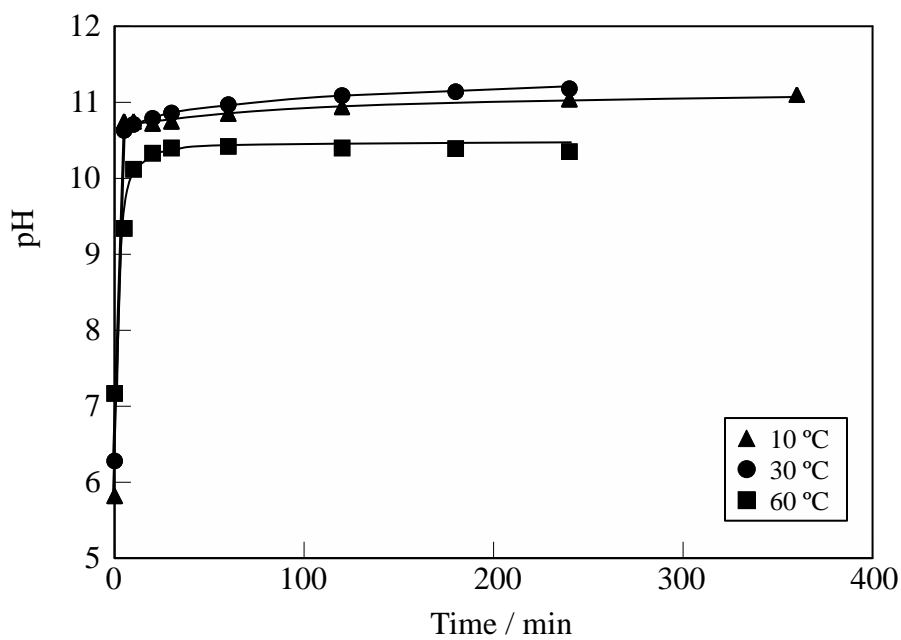


Fig. 5. Effect of temperature on pH variation during  $\text{NS}^-$  removal by the suspension of the Mg–Al oxide in  $\text{NS}^-$  solution.

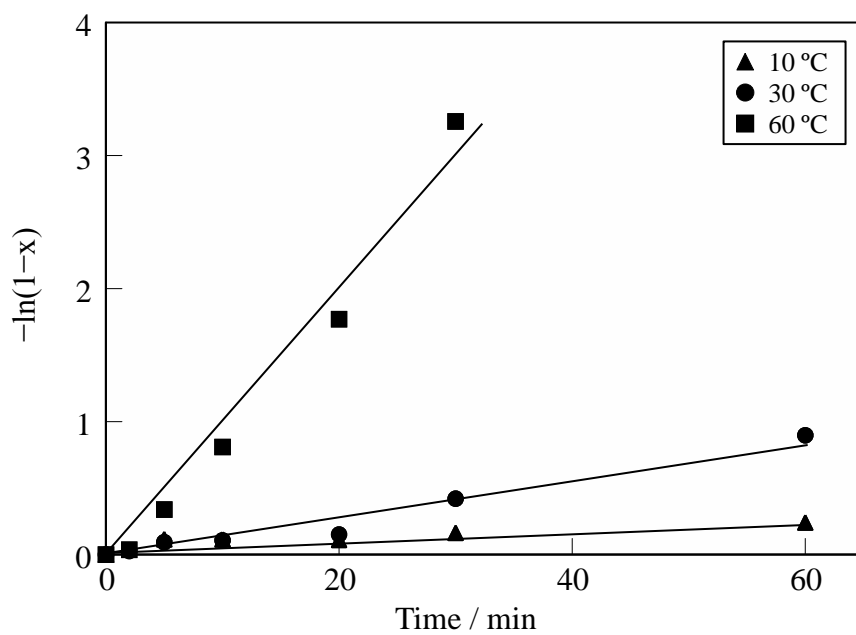


Fig. 6. Pseudo-first-order plot of  $BS^-$  removal by the suspension of the Mg–Al oxide in  $BS^-$  solution.

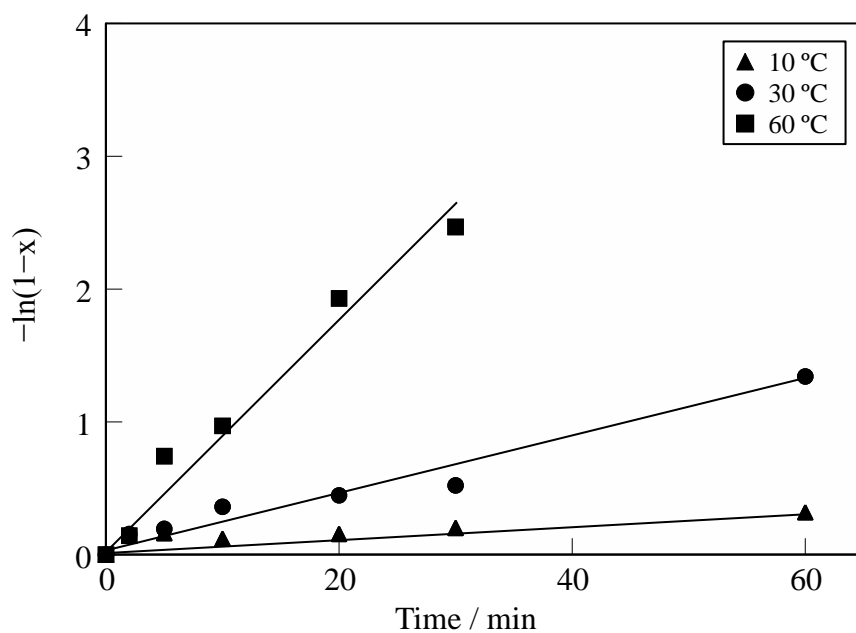


Fig. 7. Pseudo-first-order plot of NS<sup>-</sup> removal by the suspension of the Mg-Al oxide in NS<sup>-</sup> solution.

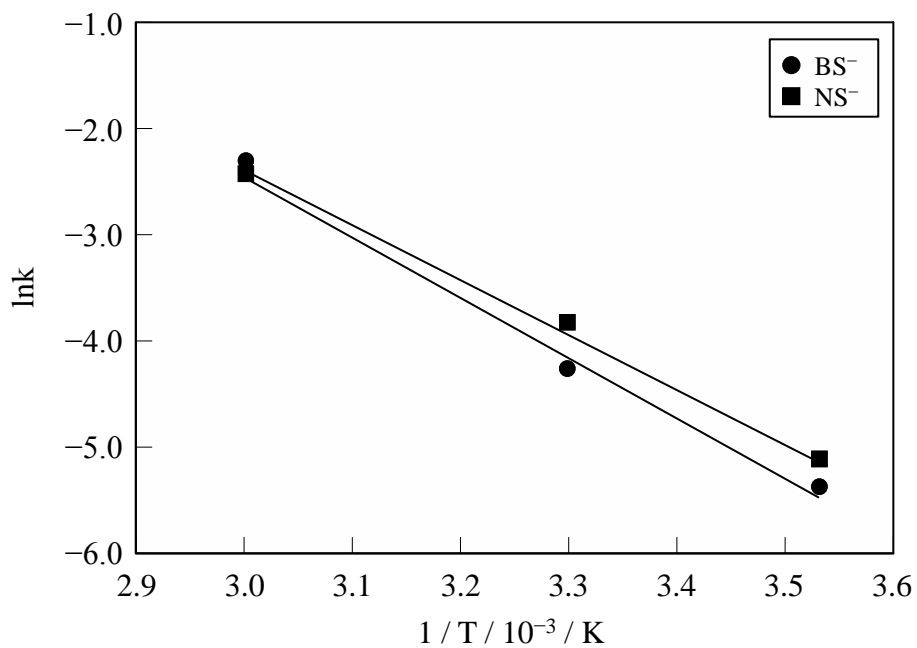


Fig. 8. Arrhenius plot of the apparent rate constant of BS<sup>-</sup> and NS<sup>-</sup> removal by the suspension of the Mg–Al oxide in BS<sup>-</sup> and NS<sup>-</sup> solutions.

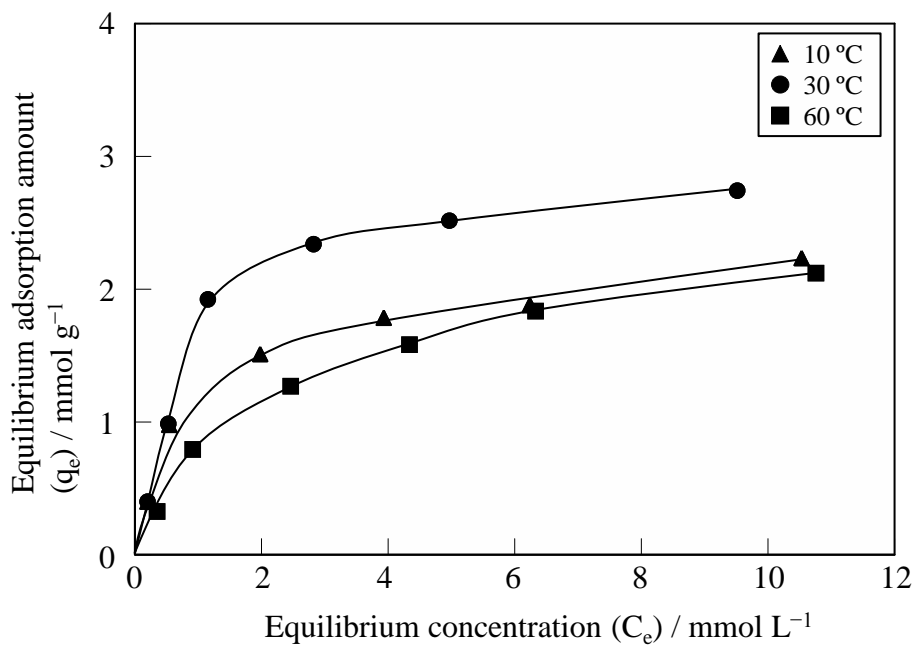


Fig. 9. Adsorption isotherm of BS<sup>-</sup> adsorbed by the Mg-Al oxide for 1440 min.

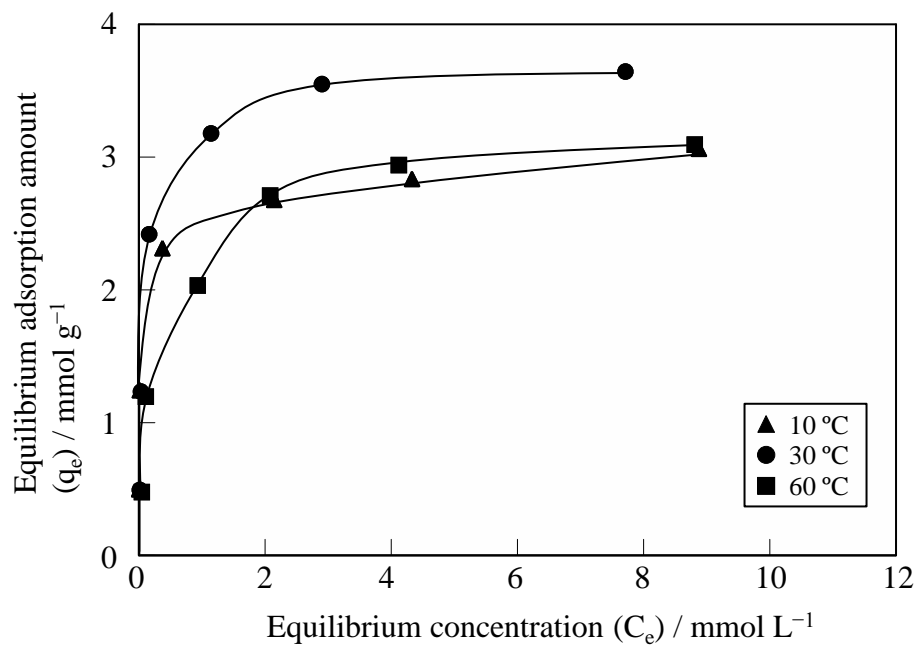


Fig. 10. Adsorption isotherm of NS<sup>-</sup> adsorbed by the Mg–Al oxide for 1440 min.

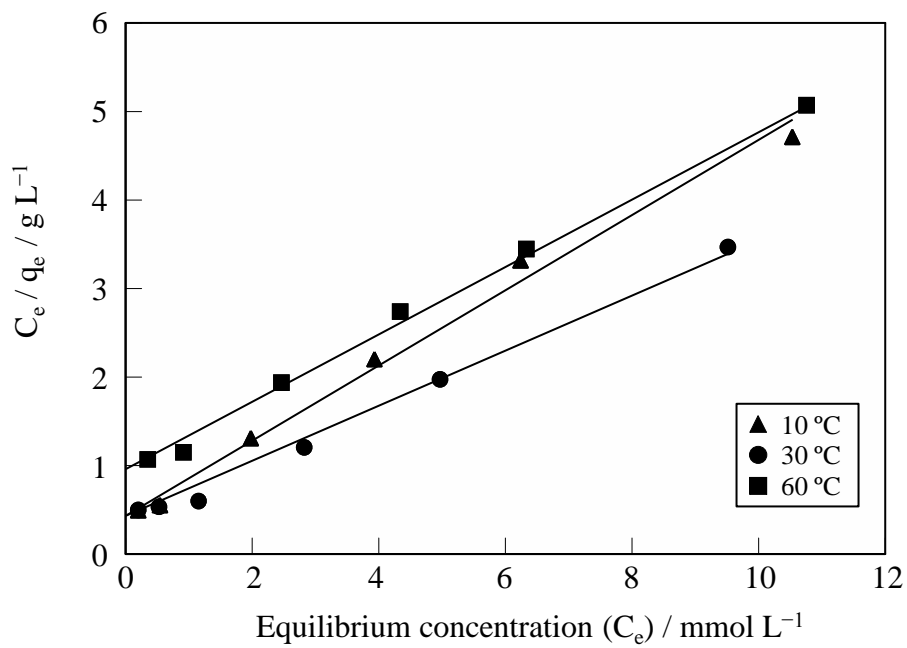


Fig. 11.  $C_e$  versus  $C_e/q_e$  plots for the adsorption isotherm of  $BS^-$  adsorbed by the Mg–Al oxide.

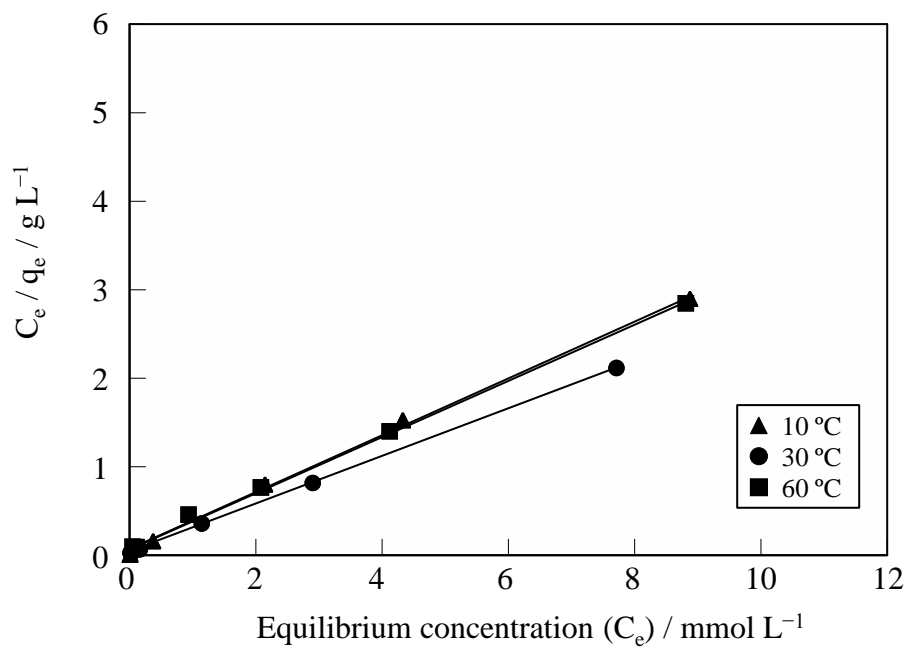


Fig. 12.  $C_e$  versus  $C_e/q_e$  plots for the adsorption isotherm of  $\text{NS}^-$  adsorbed by the Mg–Al oxide.



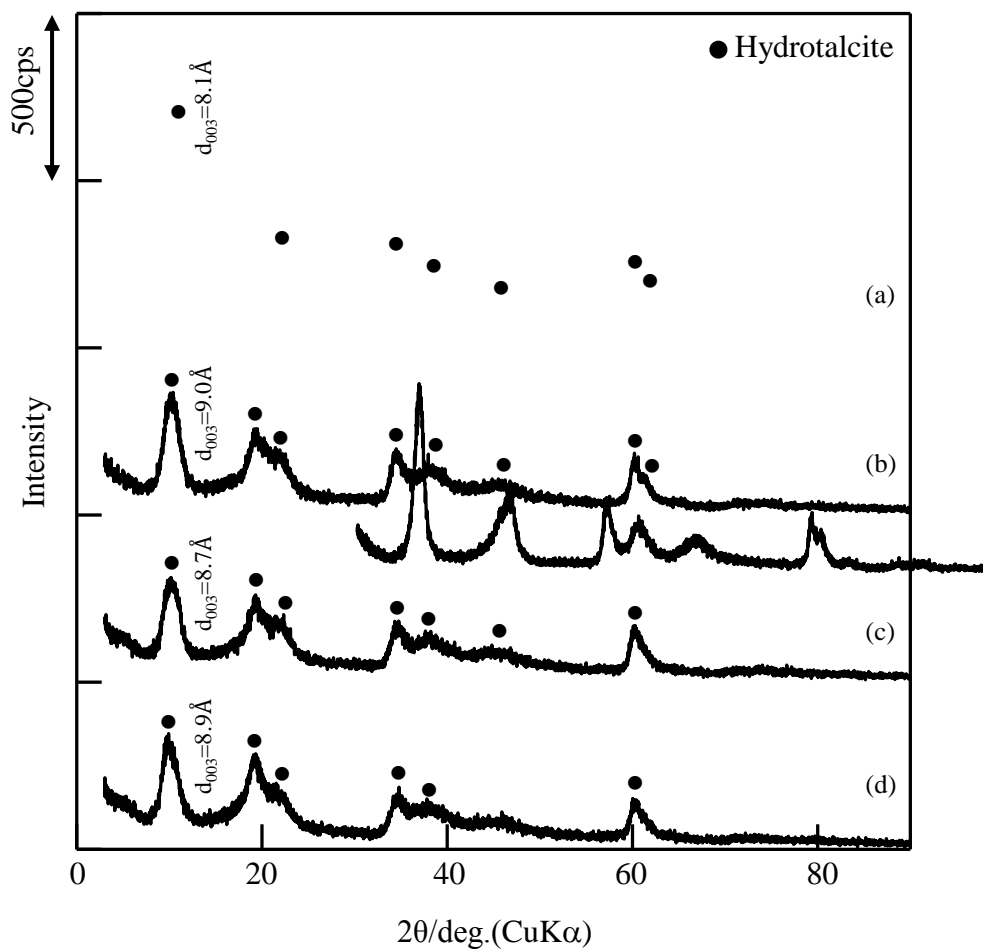


Fig. 13. XRD patterns for the products obtained by the suspension of the Mg–Al oxide in  $\text{BS}^-$  solution at 30 °C; (a)  $\text{Ce} = 0.5 \text{ mmol L}^{-1}$ , (b)  $\text{Ce} = 2.8 \text{ mmol L}^{-1}$ , (c)  $\text{Ce} = 5.0 \text{ mmol L}^{-1}$ , (d)  $\text{Ce} = 9.5 \text{ mmol L}^{-1}$ .

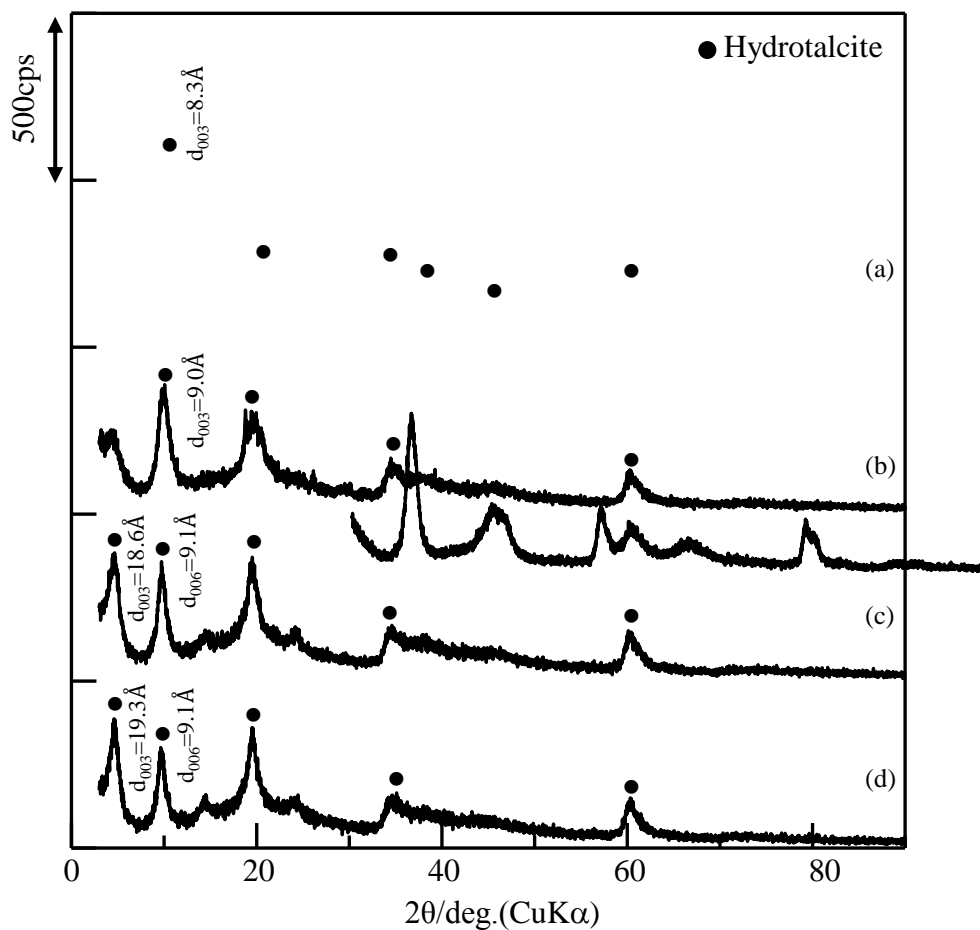


Fig. 14. XRD patterns for the products obtained by the suspension of the Mg–Al oxide in NS<sup>-</sup> solution at 30 °C; (a) Ce = 0.03 mmol L<sup>-1</sup>, (b) Ce = 1.1 mmol L<sup>-1</sup>, (c) Ce = 2.9 mmol L<sup>-1</sup>, (d) Ce = 7.7 mmol L<sup>-1</sup>.

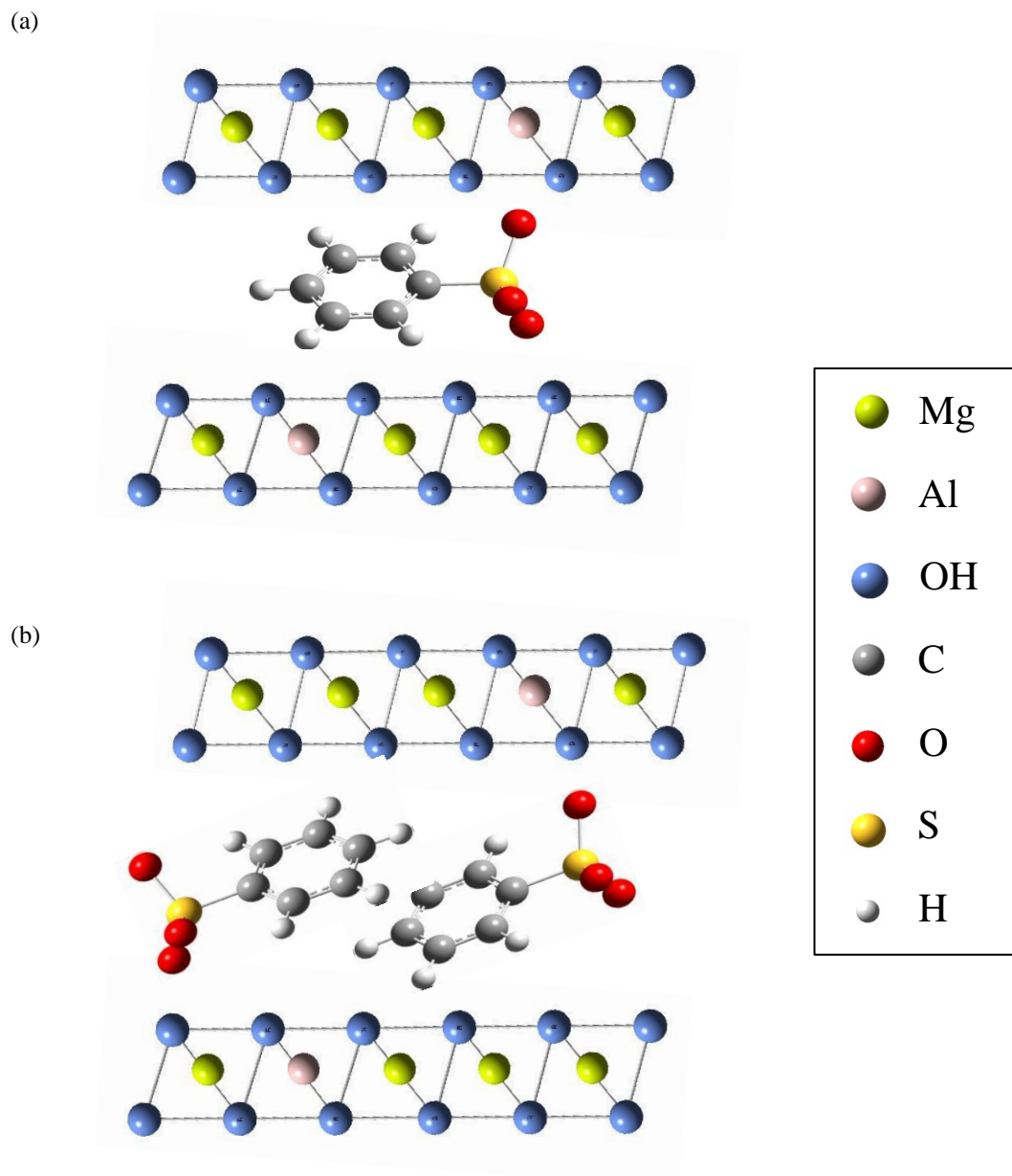


Fig. 15. Proposed molecular orientation of BS<sup>-</sup> intercalated in the interlayer of Mg–Al LDH; (a)  $C_e = 0.5 \text{ mmol L}^{-1}$ , (b)  $C_e = 2.8\text{--}9.5 \text{ mmol L}^{-1}$ .

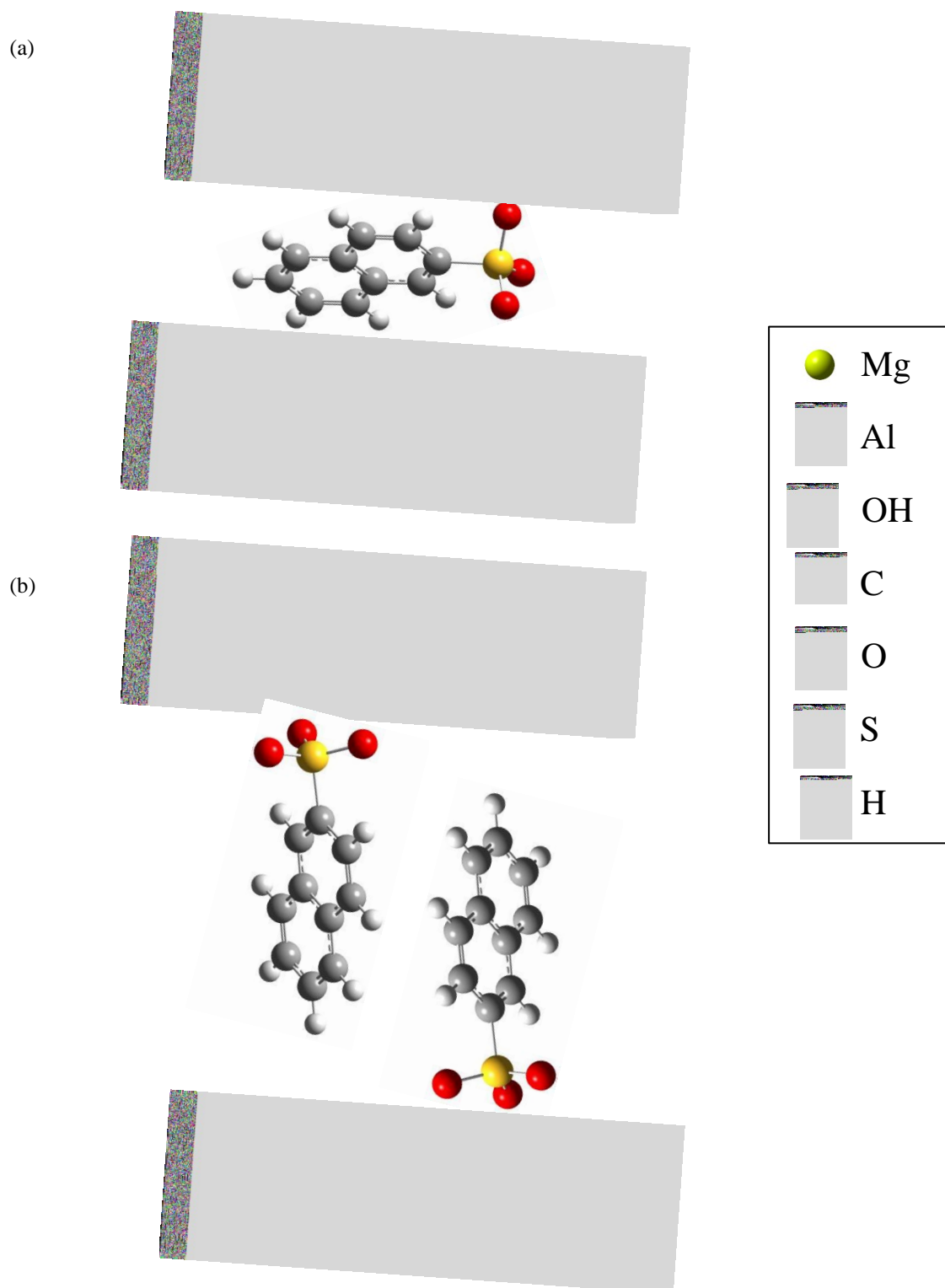


Fig. 16. Proposed molecular orientation of NS<sup>-</sup> intercalated in the interlayer of Mg–Al LDH. (a) Ce = 0.03 mmol L<sup>-1</sup>, (b) Ce = 2.9–7.7 mmol L<sup>-1</sup>.

Table 1. Equilibrium concentration and pH and relative distribution ratio ( $K$ ) after the suspension of the Mg–Al oxide in  $\text{BS}^-$  or  $\text{NS}^-$  solution.

	Equilibrium concentration/ $\text{mmol L}^{-1}$	Equilibrium pH	$K$
$\text{BS}^-$	1.6	10.9	0.14
$\text{NS}^-$	1.3	11.3	0.85

Initial  $\text{BS}^-$  or  $\text{NS}^-$  concentration:  $2 \text{ mmol L}^{-1}$ , Mg–Al oxide quantity: stoichiometric quantity, Temperature:  $30 \text{ }^\circ\text{C}$ , Time: 24 h.

Table 2. Values of  $q_m$  and  $K_L$  on  $BS^-$  and  $NS^-$  adsorbed by the Mg–Al oxide.

Adsorbate	$BS^-$			$NS^-$		
	10	30	60	10	30	60
Temperature / °C	10	30	60	10	30	60
$q_m / \text{mmol g}^{-1}$	2.4	3.1	2.6	3.1	3.7	3.2
$K_L$	0.92	0.86	0.42	7.60	9.69	2.98

Table 3.  $\text{BS}^-$  and  $\text{NS}^-$  removal by the Mg–Al oxide at 1440 min.

$\text{BS}^- / \%$			$\text{NS}^- / \%$		
10 °C	30 °C	60 °C	10 °C	30 °C	60 °C
16.6	21.5	12.9	36.7	36.6	23.3

Initial  $\text{BS}^-$  or  $\text{NS}^-$  concentration:  $2 \text{ mmol L}^{-1}$ , Mg–Al oxide quantity: stoichiometric quantity.

Table 4. pH value on  $\text{BS}^-$  and  $\text{NS}^-$  removal by the Mg–Al oxide at 1440 min.

$\text{BS}^-$			$\text{NS}^-$		
10 °C	30 °C	60 °C	10 °C	30 °C	60 °C
11.5	11.5	10.4	11.4	11.3	10.2

Initial  $\text{BS}^-$  or  $\text{NS}^-$  concentration:  $2 \text{ mmol L}^{-1}$ , Mg–Al oxide quantity: stoichiometric quantity.